Computational Condensed Matter 34 (2023) e00790

Contents lists available at ScienceDirect

Computational Condensed Matter

journal homepage: www.elsevier.com/locate/cocom

Anisotropic elastic properties of triclinic 2D materials using density functional theory with application to rhenium disulfide

Serge R. Maalouf [*,1], Senthil S. Vel [2]

University of Maine, Orono, ME 04469, USA

ARTICLE INFO

Keywords:
Anisotropic elasticity
Triclinic 2D material
Extension-shear coupling
Coefficients of mutual influence
Mechanical properties
Rhenium disulfide

ABSTRACT

In this paper, we present a rigorous and systematic approach for evaluating the linearized elastic stiffnesses of triclinic 2D materials. Unlike orthorhombic and hexagonal materials, triclinic 2D materials exhibit in-plane extension-shear coupling effects wherein axial stresses can cause a shear strain and a shear stress can induce axial strains. In the presented approach, the elastic stiffnesses of a 2D material are evaluated by curve fitting a constitutive model to either the strain energy densities or the stresses obtained for different strain states in strain space. The approach can be used to determine all the mechanical properties of a triclinic 2D material, including the coefficients of mutual influence that characterize the extension-shear coupling. The proposed approach is illustrated by evaluating the stiffness tensor of triclinic 2D rhenium disulfide using first principles calculations. The Young's and shear moduli, the Poisson's ratios and the coefficients of mutual influence of rhenium disulfide are presented along with the directional dependence of its mechanical properties. In addition, the degree of anisotropy of rhenium disulfide is discussed.

1. Introduction

Two-dimensional (2D) materials are attracting increased attention due to their salient physical properties that are advantageous in a multitude of applications such as in the semiconductor industry [1,2]. It is important to fully understand the elastic properties of 2D materials in order to use them effectively in applications [2–4]. Studies on the linear and nonlinear elastic response of 2D materials belonging to the hexagonal, orthorhombic and monoclinic symmetry classes have been published [5–15]. Triclinic 2D materials are characterized by the lack of any crystal symmetry (e.g., see [16]) and are important in applications [17,18]. Technetium diselenide, rhenium diselenide and rhenium ditelluride [10] are examples of triclinic 2D materials. Studies concerning the linear elastic response of triclinic 2D materials [19,20] and multilayer triclinic 2D materials [21] are presented in the literature. However, previous studies have focused on quantifying specific mechanical properties such as the Young's moduli and Poisson's ratios [20].

Due to the lack of symmetry, triclinic materials exhibit extension-shear coupling effects wherein axial stresses induce a shear strain and shear stresses induce normal strains (e.g., see [22]). The extension-shear coupling effects are quantified by the coefficients of mutual influence, first introduced in [23]. For orthorhombic and hexagonal materials, the coefficients of mutual influence are zero (e.g., see [5,6,16]). Although the coefficients of mutual influence appear in the theory of anisotropic elasticity [24] and have been studied for materials on the continuum scale [25,26], to the best of our knowledge, there have been no studies about the coefficients of mutual influence of triclinic 2D materials.

The mechanical properties of a triclinic 2D material, such as the coefficients of mutual influence, can be evaluated from its stiffness tensor (e.g., see [5]). The stiffness tensors and higher order elastic constants have been determined for 2D materials of higher symmetry using a polynomial based hyperelastic constitutive model [5–9,27–31]. In order to determine the elastic stiffnesses for infinitesimal deformations, we assume a quadratic polynomial hyperelastic constitutive model wherein the strain energy density is expanded as a second order polynomial in terms of the components of the strain tensor which results in linear relations between the components of the stress and strain tensors (e.g., see [32]). It is possible to evaluate the elastic stiffnesses of a triclinc 2D material by fitting its quadratic constitutive model to the strain energy densities corresponding to a set of strained states [5,6]. Alternatively, the elastic stiffnesses of a triclinc 2D material

* Corresponding author.
E-mail addresses: serge.maalouf@maine.edu (S.R. Maalouf), senthil.vel@maine.edu (S.S. Vel).
URL: https://umaine.edu/mecheng/vel/ (S.S. Vel).
[1] PhD Student in Mechanical Engineering
[2] Arthur O. Willey Professor of Mechanical Engineering

https://doi.org/10.1016/j.cocom.2023.e00790
Received 18 October 2022; Received in revised form 13 January 2023; Accepted 19 January 2023
Available online 25 January 2023

can be evaluated by fitting its linear stress–strain relations to the stresses obtained from uniaxial and shear stress simulations [7–9,27–31]. Curve fitting using the strain energy densities presents numerous advantages over stress based curve fitting in the case of nonlinear deformations [5]. In this paper we use both energy and stress based curve fitting for comparison. We illustrate the procedure by evaluating the elastic stiffnesses of triclinic 2D rhenium disulfide.

Rhenium disulfide is a triclinc 2D material belonging to the point group $P\bar{1}$ (e.g., see [33]) whose properties are favorable in applications such as logic and optoelectronic devices [4,34]. The full three-dimensional stiffness tensor of rhenium disulfide is presented in [10,35] and on the Materials Project [36–38]. The three-dimensional stiffness tensors presented in [35,37,38] correspond to that of multilayer rhenium disulfide due to the use of periodic boundary conditions with a small separation distance in the direction perpendicular to the principal material plane. The elastic properties of rhenium disulfide have been evaluated in [39], however, the relations to obtain these elastic properties and the structure of the elastic stiffnesses used correspond to that for a material of hexagonal symmetry. The nonlinear elastic response of 2D rhenium disulfide is investigated in [40] using a fifth order polynomial constitutive model, but the material is treated as a hexagonal material. There has been a lack of systematic studies to characterize the comprehensive linear elastic response of a triclinic 2D material, such as rhenium disulfide, including the coefficients of mutual influence. Furthermore, the plane stress reduced stiffness tensor of monolayer 2D rhenium disulfide has not been previously reported.

In this paper, we present an approach for determining the elastic stiffnesses of a triclinic 2D material which in-turn can be used to obtain the mechanical properties of the material, including the coefficients of mutual influence. The approach is illustrated by evaluating the plane stress reduced stiffness tensor of rhenium disulfide using plane-wave density functional theory (DFT, e.g., see [41]). The Young's moduli, shear modulus, Poisson's ratios and coefficients of mutual influence of rhenium disulfide are determined using its stiffness tensor. The variation of the directional mechanical properties of rhenium disulfide is investigated and some of its stiffnesses and moduli are compared to that published in the literature. Subsequently, we discuss the degree of anisotropy of rhenium disulfide based on its directional moduli. It is observed that the directional coefficients of mutual influence of rhenium disulfide do not collectively vanish, therefore, rhenium disulfide exhibits extension-shear coupling in the linear elastic regime, unlike any orthorhombic or hexagonal 2D material (e.g., see [5]).

2. Theoretical background

In this paper, we consider an arbitrary triclinic material as shown in Fig. 1. Triclinic materials are often studied using non-orthogonal unit cells in atomistic simulations to account for the lack of symmetry in their crystal structure (e.g., see [35,38]). However, it is also possible to analyze a triclinic material using a Cartesian coordinate system. In the present work, we analyze the materials in a global Cartesian, i.e., orthonormal, basis $\{\boldsymbol{e}_i\}$ as shown in Fig. 1 for simplicity and represent the lattice vectors in the global basis. Once the elastic stiffnesses have been evaluated in the global Cartesian basis, the Young's modulus can be determined in any direction, including the lattice parameter directions in the principal material plane. Throughout this paper, the global Cartesian basis $\{\boldsymbol{e}_i\}$ is used unless otherwise specified and the subscripts 1, 2 and 3 refer to the longitudinal direction $\boldsymbol{e}_1$, the lateral direction $\boldsymbol{e}_2$ and the out-of-plane direction $\boldsymbol{e}_3$, respectively.

2.1. Notational details

The linear elastic response of triclinic materials is studied in order to determine their elastic stiffnesses and by extension their mechanical properties. We use the Green–St. Venant strain tensor $\boldsymbol{E}$ in the present work (e.g., see [32]) since it is a rigorous strain measure that can

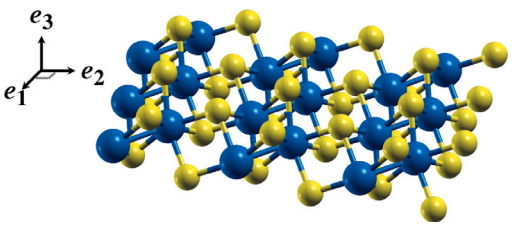

Fig. 1. A triclinic 2D material in a global Cartesian basis. The rendering of the crystal is done using XCrySDen [42].

be used to represent both linear and nonlinear strains. The Green–St. Venant strain tensor $\boldsymbol{E}$ reduces to the infinitesimal strain tensor $\boldsymbol{\varepsilon}$ in the case of infinitesimal deformations (e.g., see [32]). The Voigt contraction [43] is employed for the components of the Green–St. Venant strain tensor where,

$$E_1 = E_{11},\ E_2 = E_{22},\ E_3 = E_{33},\ E_4 = 2E_{23},\ E_5 = 2E_{13},\ E_6 = 2E_{12}. \quad (1)$$

In Eq. (1), E_{ii} represents the normal strain in the $\boldsymbol{e}_i$ direction and E_{ij} the shear strain in the $\boldsymbol{e}_i$-$\boldsymbol{e}_j$ plane. The second Piola–Kirchhoff stress tensor $\boldsymbol{S}$ is used as the stress measure (e.g., see [32]). In the case of infinitesimal deformations, the second Piola–Kirchhoff stress tensor $\boldsymbol{S}$ reduces to the Cauchy stress tensor $\boldsymbol{\sigma}$ (e.g., see [32]). We use the Voigt notation [43] for the components of the stress tensor as follows,

$$S_1 = S_{11},\ S_2 = S_{22},\ S_3 = S_{33},\ S_4 = S_{23},\ S_5 = S_{13},\ S_6 = S_{12}, \quad (2)$$

where S_{ii} represents the normal stress in the $\boldsymbol{e}_i$ direction and S_{ij} the shear stress in the $\boldsymbol{e}_i$-$\boldsymbol{e}_j$ plane. The Voigt notation and the tensorial notation are interchangeably used in this work, the difference will be clear in context. Furthermore, Einstein's summation convention (e.g., see [32]) is implied over all dummy subscript index pairs unless otherwise specified.

2.2. Constitutive model

The triclinic 2D material is analyzed using Murnaghan's hyperelastic polynomial constitutive model [44,45]. Since the deformations of interest are infinitesimal, a second order polynomial expansion of the strain energy density W in terms of the strain components is used wherein

$$W = C_i E_i + \frac{1}{2} C_{ij} E_i E_j, \quad (3)$$

where C_i and C_{ij} are elastic constants and the subscript indices i and j vary in $\{1,2,3,4,5,6\}$. The stress components are obtained using Eq. (3) and the hyperelastic constitutive relations in an orthonormal basis (e.g., see [32]) as follows,

$$S_i = \frac{\partial W}{\partial E_i} = C_i + C_{ij} E_j. \quad (4)$$

In the present work, we do not consider prestressed 2D materials, thus, $\boldsymbol{S} = \boldsymbol{0}$ when $\boldsymbol{E} = \boldsymbol{0}$ which implies that $C_i = 0$ for all $i \in \{1,2,3,4,5,6\}$. Furthermore, we study 2D materials under plane stress conditions (e.g., see [5,6]), i.e., $S_3 = S_4 = S_5 = 0$. Therefore, the strain energy density can be expressed in terms of three of the six strain components, e.g., the longitudinal axial strain E_1, the lateral axial strain E_2 and the in-plane shear strain E_6. Consequently,

$$W = \frac{1}{2} Q_{ij} E_i E_j, \quad (5)$$

where Q_{ij} are the plane stress reduced elastic constants and the subscript indices i and j vary now in $\{1,2,6\}$. It follows from Eqs. (4) and (5) that

$$S_i = Q_{ij} E_j, \quad (6)$$

which represents the linearized stress–strain relations under plane stress conditions (e.g., see [32]). The plane stress reduced elastic

constants Q_{ij} will be referred to as just elastic constants or elastic stiffnesses hereinafter for simplicity. It is noted that the elastic stiffnesses satisfy the symmetry relation $Q_{ij} = Q_{ji}$ for all $i, j \in \{1, 2, 6\}$ (e.g., see [5]).

2.3. Mechanical properties of triclinic 2D materials

The stress–strain relations shown in Eq. (6) can be written in expanded form as

$$\begin{Bmatrix} S_1 \\ S_2 \\ S_6 \end{Bmatrix} = \begin{bmatrix} Q_{11} & Q_{12} & Q_{16} \\ Q_{12} & Q_{22} & Q_{26} \\ Q_{16} & Q_{26} & Q_{66} \end{bmatrix} \begin{Bmatrix} E_1 \\ E_2 \\ E_6 \end{Bmatrix}. \tag{7}$$

Eq. (7) can be inverted to obtain the compliance relations and by extension the mechanical properties of a triclinic 2D material as follows (e.g., see [5]),

$$\begin{Bmatrix} E_1 \\ E_2 \\ E_6 \end{Bmatrix} = \begin{bmatrix} Q_{11} & Q_{12} & Q_{16} \\ Q_{12} & Q_{22} & Q_{26} \\ Q_{16} & Q_{26} & Q_{66} \end{bmatrix}^{-1} \begin{Bmatrix} S_1 \\ S_2 \\ S_6 \end{Bmatrix} = \begin{bmatrix} \frac{1}{Y_1} & -\frac{\nu_{21}}{Y_2} & \frac{\eta_{16}}{G} \\ -\frac{\nu_{12}}{Y_1} & \frac{1}{Y_2} & \frac{\eta_{26}}{G} \\ \frac{\eta_{61}}{Y_1} & \frac{\eta_{62}}{Y_2} & \frac{1}{G} \end{bmatrix} \begin{Bmatrix} S_1 \\ S_2 \\ S_6 \end{Bmatrix}, \tag{8}$$

where Y_i represents the Young's modulus in the $\boldsymbol{e_i}$ direction, G is the shear modulus in the $\boldsymbol{e_1}$-$\boldsymbol{e_2}$ plane, ν_{12} and ν_{21} are the Poisson's ratios in the $\boldsymbol{e_1}$-$\boldsymbol{e_2}$ plane, η_{i6} are the coefficients of mutual influence of the first kind and η_{6i} are the coefficients of mutual influence of the second kind. The Poisson's ratio ν_{12} is the negative of the ratio of the lateral strain E_2 to the longitudinal strain E_1 when the material is only subjected to an axial stress S_1. In comparison, ν_{21} is defined as the negative of the ratio of the longitudinal strain E_1 to the lateral strain E_2 when the material is only subjected to an axial lateral stress S_2. In general for an anisotropic material, $\nu_{12} \neq \nu_{21}$ but they are related through the reciprocity relation (e.g., see [32])

$$\frac{\nu_{12}}{Y_1} = \frac{\nu_{21}}{Y_2}, \tag{9}$$

which follows from the symmetry of the elastic stiffnesses. Triclinic materials also exhibit extension-shear coupling wherein a shear stress S_6 will induce normal strains E_1 and E_2 which are quantified by the coefficients of mutual influence of the first kind η_{16} and η_{26}, respectively. Similarly, a normal stress S_1 or S_2 will induce a shear strain E_6 which is quantified by the coefficients of mutual influence of the second kind η_{61} and η_{62}, respectively. Since the stiffness matrix $\boldsymbol{Q}$ is symmetric, the coefficients of mutual influence satisfy the following relations,

$$\frac{\eta_{61}}{Y_1} = \frac{\eta_{16}}{G} \quad \text{and} \quad \frac{\eta_{62}}{Y_2} = \frac{\eta_{26}}{G}. \tag{10}$$

As shown in Eq. (8), the closed form expressions for the mechanical properties are obtained by taking the inverse of a stiffness tensor $\boldsymbol{Q}$ as follows,

$$\begin{aligned}
Y_1 &= Q_{11} - \frac{Q_{12}^2}{Q_{22}} - \frac{\left(Q_{16}Q_{22} - Q_{12}Q_{26}\right)^2}{Q_{22}\left(Q_{22}Q_{66} - Q_{26}^2\right)}, \\
Y_2 &= Q_{22} - \frac{Q_{12}^2}{Q_{11}} - \frac{\left(Q_{12}Q_{16} - Q_{11}Q_{26}\right)^2}{Q_{11}\left(Q_{11}Q_{66} - Q_{16}^2\right)}, \\
G &= Q_{66} + \frac{Q_{22}Q_{16}^2 - 2Q_{12}Q_{16}Q_{26} + Q_{11}Q_{26}^2}{Q_{12}^2 - Q_{11}Q_{22}}, \\
\nu_{12} &= \frac{Q_{12}}{Q_{22}} + \frac{Q_{26}\left(Q_{12}Q_{26} - Q_{22}Q_{16}\right)}{Q_{22}\left(Q_{22}Q_{66} - Q_{26}^2\right)}, \\
\eta_{16} &= \frac{Q_{22}Q_{16} - Q_{12}Q_{26}}{Q_{12}^2 - Q_{11}Q_{22}}, \\
\eta_{26} &= \frac{Q_{11}Q_{26} - Q_{12}Q_{16}}{Q_{12}^2 - Q_{11}Q_{22}},
\end{aligned} \tag{11}$$

where the remaining Poisson's ratio ν_{21} and coefficients of mutual influence η_{61} and η_{62} can be determined using Eqs. (9) and (10), respectively. It is noted that by comparison with the expressions for the mechanical properties of an orthorhombic material (e.g., see [5]), the last summand in each of the expressions presented in Eq. (11) accounts for the anisotropy of a triclinic material. The latter terms, in addition to η_{16} and η_{26}, relate to extension-shear coupling and will vanish if $Q_{16} = Q_{26} = 0$ which is the case for any higher symmetry class.

2.4. Evaluating the elastic stiffnesses

The elastic constants Q_{ij} of a triclinic 2D material can be evaluated by curve fitting the constitutive model presented in Eq. (5) to the strain energy densities obtained using density functional theory. Alternatively, the elastic constants Q_{ij} can be evaluated by curve fitting the stress–strain relations shown in Eq. (6) to the stresses determined using density functional theory. We present and use both approaches for comparison purposes.

2.4.1. Curve fitting using the strain energy densities

In order to evaluate the elastic constants Q_{ij} of a triclinic material using the strain energy densities we use the ray based methodology [5, 6] which is based on curve fitting the polynomial constitutive model shown in Eq. (5) to the strain energy densities corresponding to a multitude of strain states sampled along rays in strain space.

We first define strain space as the space spanned by the scalars E_1, E_2 and E_6. Each point in strain space corresponds to a specific strain state as defined by the values of the longitudinal normal strain E_1, lateral normal strain E_2 and shear strain E_6. We sample points along rays in strain space to curve fit for the elastic constants of a triclinic 2D material and we limit our sampling region to a sphere of radius R centered at the origin (e.g., see [5]). Since a ray's direction can be uniquely defined using the ray's azimuthal angle θ and polar angle ϕ, the components of a strain state on a ray can be written in Voigt notation as

$$\begin{cases} E_1 = r\cos\theta\sin\phi, \\ E_2 = r\sin\theta\sin\phi, \\ E_6 = r\cos\phi, \end{cases} \tag{12}$$

where r denotes the Euclidean norm (e.g., see [5]). For each strain state, the strain energy density is computed using atomistic simulations. In this work, we employ density functional theory [46,47].

The first step in evaluating the elastic constants of a material using the ray based methodology is to choose a set of sampling rays by defining their directions θ and ϕ, in addition to the strain states on each ray defined by their norms r. We consider that $\mathcal{M}$ sampling rays are used with $\mathcal{N}$ equidistant strain states on each ray excluding the origin. We can index our strain states using 2 integers i and j representing the ray number and the strain state on the ray, respectively. Thus, $i \in \{1, 2, \ldots, \mathcal{M}\}$ and $j \in \{1, 2, \ldots, \mathcal{N}\}$. A sample strain tensor $\boldsymbol{E}^{(i,j)}$ can be written in Voigt notation as

$$\begin{Bmatrix} E_1^{(i,j)} \\ E_2^{(i,j)} \\ E_6^{(i,j)} \end{Bmatrix} = j\frac{R}{\mathcal{N}} \begin{Bmatrix} \cos\theta_i\sin\phi_i \\ \sin\theta_i\sin\phi_i \\ \cos\phi_i \end{Bmatrix}, \tag{13}$$

where θ_i and ϕ_i are the azimuthal angle and polar angle of the ith ray, respectively. The second step in the ray based methodology is to compute the strain energy density $W^{(i,j)}$ corresponding to the strain state $\boldsymbol{E}^{(i,j)}$ for all i and j. We do so using plane-wave density functional theory as follows,

$$W^{(i,j)} = \frac{1}{\Omega}\left(\mathcal{E}^{(i,j)} - \mathcal{E}^{(0,0)}\right), \tag{14}$$

where Ω is the ground state area of the system (to obtain stiffnesses in N/m, e.g., see [5]), $\mathcal{E}^{(i,j)}$ is the total energy of the material subjected to the strain tensor $\boldsymbol{E}^{(i,j)}$ and $\mathcal{E}^{(0,0)}$ is the ground state energy of the system. In order to determine $\mathcal{E}^{(i,j)}$ using density functional theory, we deform the material unit cell following the deformation gradient

$\boldsymbol{F}^{(i,j)}$ corresponding to the strain $\boldsymbol{E}^{(i,j)}$. To obtain the upper triangular deformation gradient $\boldsymbol{F}^{(i,j)}$ corresponding to the strain tensor $\boldsymbol{E}^{(i,j)}$, we use the Cholesky decomposition (e.g., see [48,49]) of

$$2\boldsymbol{E}^{(i,j)} - \boldsymbol{I} = \boldsymbol{F}^{(i,j)^T}\boldsymbol{F}^{(i,j)}, \tag{15}$$

where $\boldsymbol{I}$ is the identity tensor. The Cholesky decomposition shown in Eq. (15) exists since by definition, $2\boldsymbol{E} - \boldsymbol{I} = \boldsymbol{F}^T\boldsymbol{F}$ and $\boldsymbol{F}^T\boldsymbol{F}$ is symmetric positive-definite (e.g., see [48]). In the case of two-dimensional deformations, the strain tensor $\boldsymbol{E}^{(i,j)}$ is represented by a 2×2 matrix, therefore the deformation gradient $\boldsymbol{F}^{(i,j)}$, obtained through Cholesky decomposition, is,

$$\boldsymbol{F}^{(i,j)} = \begin{bmatrix} \sqrt{2E_1^{(i,j)} + 1} & \dfrac{E_6^{(i,j)}}{\sqrt{2E_1^{(i,j)} + 1}} \\ 0 & \sqrt{2E_2^{(i,j)} + 1 - \dfrac{{E_6^{(i,j)}}^2}{2E_1^{(i,j)} + 1}} \end{bmatrix}. \tag{16}$$

It is noted that $2E_1+1 > 0$ for any physically allowable strain state since otherwise the deformation would correspond to an area collapsing into a line (e.g., see [32]).

We define $\mathscr{L}$ as the matrix in which each column corresponds to the components of the in-plane lattice vectors of the unit cell in the $\{\boldsymbol{e}_i\}$ basis, i.e.,

$$\mathscr{L} = \begin{bmatrix} l_1^{(1)} & l_1^{(2)} \\ l_2^{(1)} & l_2^{(2)} \end{bmatrix}, \tag{17}$$

where $\boldsymbol{l}^{(i)}$ are the in-plane lattice vectors defining the unit cell being simulated. The deformation can be applied as follows,

$$\mathscr{L}^{(i,j)} = \boldsymbol{F}^{(i,j)}\mathscr{L}^{(0,0)}, \tag{18}$$

where $\mathscr{L}^{(i,j)}$ is the deformed lattices matrix and $\mathscr{L}^{(0,0)}$ is the matrix of ground state lattice parameters. After the lattice vectors are deformed to that corresponding to $\mathscr{L}^{(i,j)}$, the atomic coordinates are relaxed to reach the local minimum energy configuration of the material and obtain $\mathcal{E}^{(i,j)}$.

Finally, after sampling for the strain energy densities, we use linear least squares (e.g., see [50]) to globally curve fit and determine the elastic constants [5] using (e.g., see [50,51])

$$\begin{bmatrix} Q_{11} & Q_{22} & Q_{66} & Q_{12} & Q_{16} & Q_{26} \end{bmatrix}^T = \left(\boldsymbol{B}^T\boldsymbol{B}\right)^{-1}\left(\boldsymbol{B}^T\boldsymbol{W}\right), \tag{19}$$

where using the injective map $\mathcal{I} = \mathcal{N}(i-1)+j$, $\boldsymbol{W}$ is the vector defined using each (i,j) pair as

$$W_{\mathcal{I}} = W^{(i,j)}, \tag{20}$$

and the rows of the matrix $\boldsymbol{B}$ are defined as,

$$B_{\mathcal{I},1\ldots6} = \begin{bmatrix} \frac{1}{2}E_1^{(i,j)^2} & \frac{1}{2}E_2^{(i,j)^2} & \frac{1}{2}E_6^{(i,j)^2} & E_1^{(i,j)} \cdot E_2^{(i,j)} & E_1^{(i,j)} \cdot E_6^{(i,j)} & E_2^{(i,j)} \cdot E_6^{(i,j)} \end{bmatrix}. \tag{21}$$

More rays are added as necessary to increase the accuracy of the elastic constants.

2.4.2. Curve fitting using the stresses

The elastic constants Q_{ij} can also be determined using the stresses corresponding to different strain states similarly to how this is done in [7]. We can determine, using linear least squares (e.g., see [50,51]), the ith column of the stiffness tensor using simulations where $E_i \neq 0$ for some $i \in \{1,2,6\}$ and $E_j = E_k = 0$ for $j,k \in \{1,2,6\}$, $j \neq k$ and $j,k \neq i$ as follows,

$$Q_{ij} = \left(\boldsymbol{\mathcal{B}}^T\boldsymbol{\mathcal{B}}\right)^{-1}\left(\boldsymbol{\mathcal{B}}^T\boldsymbol{S}_j\right), \tag{22}$$

where $\boldsymbol{\mathcal{B}}$ is the column vector containing the applied strains E_i and $\boldsymbol{S}_j$ is the column vector containing the corresponding stress components S_j, in the same order, computed using density functional theory. It is noted that similarly to the ray based methodology, for a given strain state the deformation gradient is determined using Cholesky decomposition as in Eq. (16) and the unit cell is deformed accordingly following Eq. (18) and the atomic coordinates relaxed to obtain the stresses.

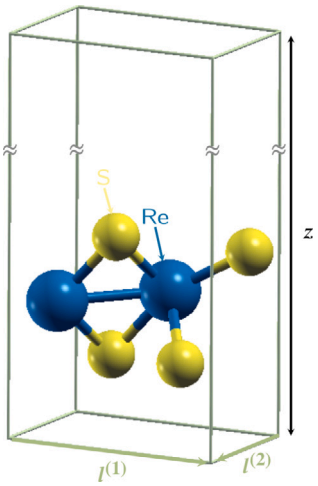

Fig. 2. Six-atom rhenium disulfide unit cell used in the density functional theory calculations. The rendering of the crystal is done using XCrySDen [42].

Table 1
Converged values of the parameters used in the Quantum-Espresso calculations.

Parameter	Value used
K_x, K_y	14
K_z	2
Total energy convergence threshold	10^{-9} Ry
Electron energy convergence threshold	10^{-10} Ry
Force convergence threshold	10^{-6} eV/Å
Kinetic energy cut-off	150 Ry
z lattice vector dimension	20 Å

3. Computational details

We illustrate the methodology presented in Section 2 by evaluating the elastic stiffnesses of rhenium disulfide which is a triclinic 2D material. We calculate the energies and the stresses of different rhenium disulfide configurations using plane-wave density functional theory [46,47] employing the open source software Quantum-Espresso [52,53]. Projector augmented wave pseudopotentials [54] and the Perdew–Burke–Ernzerhof generalized gradient approximation [55] are used. In order to determine the Quantum-Espresso parameters to be used in the simulations, a convergence analysis is carried out which consists of relaxing the six-atom rhenium disulfide unit cell shown in Fig. 2, where the in-plane lattice vectors $\boldsymbol{l}^{(1)}$ and $\boldsymbol{l}^{(2)}$ and the atomic coordinates are allowed to change to reach the ground state configuration. The ground state energy as well as the components of the in-plane lattice vectors are then compared for different values of each parameter to assess convergence. It is noted that the parameter z shown in Fig. 2 is studied and chosen to avoid any interactions between adjacent cells of rhenium disulfide in the out-of-plane direction. The corresponding out-of-plane lattice vector, which is orthogonal to the $\boldsymbol{e_1}$-$\boldsymbol{e_2}$ plane, remains unchanged in the simulations since we are studying single layer rhenium disulfide.

The converged values that are used in all the simulations are presented in Table 1. K_x, K_y and K_z represent the Monkhorst–Pack K-space discretization [56] in each reciprocal space direction, respectively.

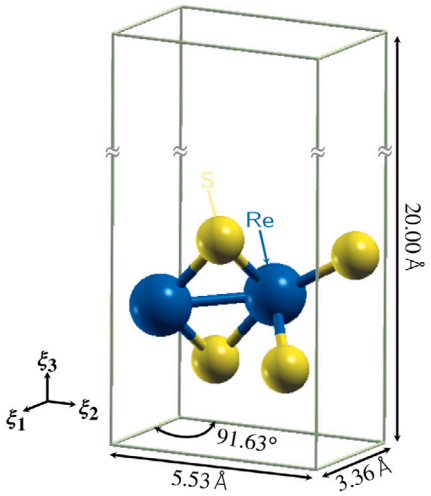

(a) Ground state unit cell of rhenium disulfide used in the density functional theory calculations

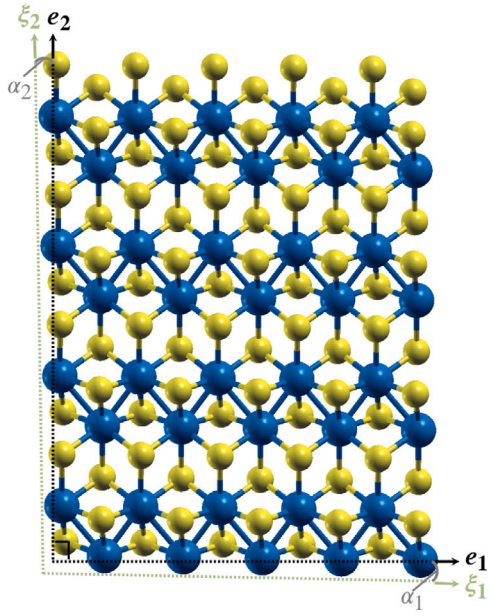

(b) Top view of rhenium disulfide showing the global orthonormal coordinate system $\{e_i\}$ and the non-orthogonal cell coordinate system $\{\xi_i\}$. $\alpha_1 = 0.818°$ and $\alpha_2 = 0.808°$

Fig. 3. Ground state geometry and unit cell of rhenium disulfide. The rendering of the crystals is done using XCrySDen [42].

4. Ground state configuration of rhenium disulfide

Using the Quantum-Espresso parameters presented in Table 1, we perform a unit cell energy minimization to obtain the ground state configuration of rhenium disulfide. Fig. 3(a) shows the ground state unit cell in the unit cell coordinate system $\{\xi_i\}$. The unit cell coordinate system $\{\xi_i\}$ is oriented along the lattice vectors and is not Cartesian since ξ_1 and ξ_2 are not orthogonal. Indeed, the ground state lattice parameters matrix of rhenium disulfide $\mathscr{L}^{(0,0)}$ in the $\{e_i\}$ basis is given by,

$$\mathscr{L}^{(0,0)} = \begin{bmatrix} 3.363 & -0.078 \\ -0.048 & 5.528 \end{bmatrix} (\text{Å}). \tag{23}$$

Fig. 3(b) shows the top view of the ground state configuration of rhenium disulfide, along with the global and unit cell bases directions. As can be seen in Fig. 3(b), the ξ_1 unit cell basis vector is at an angle of $\alpha_1 = -0.818°$ relative to the global basis vector e_1 and the unit cell basis vector ξ_2 is at an angle of $\alpha_2 = 0.808°$ relative to the global basis vector e_2.

For computational convenience, we use six atoms in the unit cell for our density functional theory simulations (cf. Fig. 3(a)) based on the minimum number of atoms in a 2D rhenium disulfide conventional unit cell [38,57]. The in-plane angle between the ξ_1 and ξ_2 axes in this work is approximately 92° as shown in Fig. 3(a), whereas in other conventional unit cells presented in the literature this angle is closer to 120° [10,38,57]. While different conventional unit cells can be used to study the same periodic system (e.g., see [41]) the resulting elastic stiffnesses in the chosen global basis $\{e_i\}$ should remain unaffected.

5. Elastic constants of rhenium disulfide

We evaluate the elastic constants of rhenium disulfide using density functional theory. We present the results obtained using both stress and energy based curve fitting for comparison (cf. Section 2.4).

Table 2
Ray directions used to sample for the strain energy density of rhenium disulfide in strain space.

Elastic constant	$\theta(°/180)$	$\phi(°/180)$
Q_{11}	$\{0,1\}$	$1/2$
Q_{22}	$\pm 1/2$	$1/2$
Q_{66}	0	$\{0,1\}$
Q_{12}	$\pm\{1/4, 3/4\}$	$1/2$
Q_{16}	$\{0,1\}$	$\{n/8 \mid n \in \{1,2,3,5,6,7\}\}$
Q_{26}	$\pm 1/2$	$\{n/8 \mid n \in \{1,2,3,5,6,7\}\}$

5.1. Curve fitting using the energies

We choose the ray directions shown in Table 2 to evaluate the elastic stiffnesses of rhenium disulfide using the ray based methodology [5]. It is noted that more rays are used in the E_1-E_6 and E_2-E_6 planes of strain space since Q_{16} and Q_{26} are smaller than the other stiffnesses and therefore are more sensitive to small numerical differences.

Furthermore, we consider $\mathcal{N} = 4$ equidistant strain states on each ray and the strain ball of radius $R = 2 \times 10^{-3} = 0.2\%$, chosen within the linear elastic regime. To ensure that the elastic stiffnesses evaluated using curve fitting are accurate based on the number points per ray chosen, we evaluate these elastic constants using 1, 2 and 4 equidistant points per ray with the same 34 rays shown in Table 2. Furthermore, to assess if the number of rays used is sufficient we perform the same evaluations using 18 rays for comparison. The elastic constants obtained from these analyses are presented in Table 3. As can be seen in Table 3, the elastic constants evaluated using different numbers of rays and points per ray are nearly identical. Therefore, it is concluded that the 34 rays shown in Table 2 with 4 points per ray are sufficient to accurately determine the elastic constants of rhenium disulfide.

Table 3
Elastic stiffnesses of rhenium disulfide obtained using 18 and 34 rays and 1, 2 and 4 equidistant points per ray to assess their accuracy.

Number of rays $\mathcal{M}$	18			34		
Number of points per ray $\mathcal{N}$	1	2	4	1	2	4
Q_{11} (N/m)	104.6	104.6	104.6	104.6	104.6	104.6
Q_{22} (N/m)	144.5	144.5	144.6	144.5	144.5	144.6
Q_{66} (N/m)	47.4	47.5	47.5	47.4	47.5	47.5
Q_{12} (N/m)	27.4	27.4	27.4	27.4	27.4	27.4
Q_{16} (N/m)	6.9	6.9	6.9	6.9	6.8	6.8
Q_{26} (N/m)	1.3	1.3	1.3	1.3	1.3	1.3

The elastic constants obtained using energy based curve fitting are presented in the stiffness tensor

$$\boldsymbol{Q}^{(\mathrm{W})} = \begin{bmatrix} 104.6 & 27.4 & 6.8 \\ 27.4 & 144.6 & 1.3 \\ 6.8 & 1.3 & 47.5 \end{bmatrix} (\mathrm{N/m}), \tag{24}$$

where the superscript (W) represents curve fitting using the energies. The global root mean square error in the curve fit used to determine the elastic constants shown in Eq. (24) is 1.99×10^{-5} J/m^2.

5.2. Curve fitting using the stresses

In order to curve fit for the stiffnesses of rhenium disulfide using the stresses, we run density functional theory simulations with $\mathcal{N} = 4$ equidistant strain states per simulation. The simulations performed consist of applying respectively tensile and compressive axial strains E_1 and E_2 and positive and negative shear strains E_6. The elastic constants obtained using stress based curve fitting are presented in the stiffness tensor

$$\boldsymbol{Q}^{(\mathrm{S})} = \begin{bmatrix} 103.9 & 26.8 & 6.9 \\ 26.9 & 143.9 & 1.8 \\ 6.8 & 1.4 & 47.5 \end{bmatrix} (\mathrm{N/m}), \tag{25}$$

where the superscript (S) represents curve fitting using the stresses. As can be seen in Eq. (25), curve fitting using the stresses does not result in a perfectly symmetric stiffness tensor $\boldsymbol{Q}$ due to minor differences in the density functional theory stresses corresponding to different simulations, e.g., S_6 from an E_1 simulation and S_1 from an E_6 simulation. The elastic constant Q_{26} varies the most since it is smaller than the other elastic constants and thus the most sensible to minor variations in the data used for the curve fitting.

5.3. Discussion

There exist some differences between the components of the stiffness tensors $\boldsymbol{Q}^{(\mathrm{W})}$ and $\boldsymbol{Q}^{(\mathrm{S})}$. Furthermore, $\boldsymbol{Q}^{(\mathrm{S})}$ is not symmetric which violates the symmetry of the stiffness tensor shown in Eq. (8). The stresses, which are obtained from the derivatives of the energy with respect to the strains in density functional theory [58], are less accurate than the corresponding energies since differentiation increases computational inaccuracies. Furthermore, more rays, i.e., simulations, are used for the curve fitting using the ray based methodology, which accounts for a larger number of strain states. Therefore, the stiffnesses obtained using the proposed energy based curve fitting method more accurately describe the elastic response of rhenium disulfide when subjected to different strain states in the chosen strain space sphere than those obtained using stress based curve fitting. Therefore, we conclude that $\boldsymbol{Q}^{(\mathrm{W})}$ is more accurate than $\boldsymbol{Q}^{(\mathrm{S})}$, especially since $\boldsymbol{Q}^{(\mathrm{W})}$ is symmetric. Stress based curve fitting is a more efficient option since it only required 6 simulations instead of 34. Therefore, in studies that do not require high accuracy, stress based curve fitting can be used but the symmetry of the tensor has to be enforced. We use $\boldsymbol{Q} = \boldsymbol{Q}^{(\mathrm{W})}$ for the subsequent analyses as the stiffness tensor of rhenium disulfide.

Table 4
Mechanical properties of rhenium disulfide obtained using its elastic stiffness tensor.

Y_1 (N/m)	Y_2 (N/m)	G (N/m)	ν_{12}	ν_{21}	η_{16}	η_{61}	η_{26}	η_{62}
98.5	137.4	47.1	0.188	0.263	−0.066	−0.138	0.004	0.010

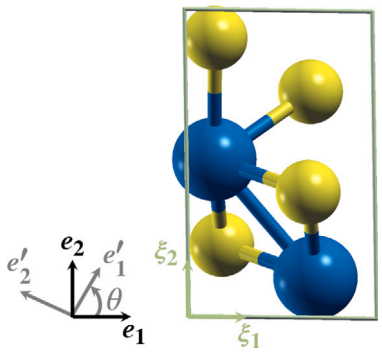

Fig. 4. Rotated global coordinate system $\{e'_i\}$ used to analyze rhenium disulfide. The rendering of the crystal is done using XCrySDen [42].

6. Mechanical properties of rhenium disulfide

The mechanical properties of rhenium disulfide obtained from the stiffness tensor presented in Eq. (24) and the relations shown in Eq. (8) are presented in Table 4.

6.1. Directional mechanical properties

It is of interest to analyze the directional variation of the mechanical properties of rhenium disulfide. This is achieved by utilizing the rotated coordinate system $\{e'_i\}$ oriented at an angle θ relative to the $\{e_i\}$ basis, as shown in Fig. 4.

It is possible to obtain the stiffness tensor of rhenium disulfide, in Voigt notation, in the rotated coordinate system as follows [59]

$$\boldsymbol{Q}(\theta) = \boldsymbol{\Gamma}\,\boldsymbol{Q}\,\boldsymbol{\Gamma}^T, \tag{26}$$

where

$$\boldsymbol{\Gamma} = \begin{bmatrix} \cos^2\theta & \sin^2\theta & 2\cos\theta\sin\theta \\ \sin^2\theta & \cos^2\theta & -2\cos\theta\sin\theta \\ -\cos\theta\sin\theta & \cos\theta\sin\theta & \cos^2\theta - \sin^2\theta \end{bmatrix}, \tag{27}$$

$\boldsymbol{Q}(\theta)$ is the stiffness tensor in the coordinate system $\{e'_i\}$ and $\boldsymbol{Q}$ is presented in Eq. (24). Using the transformation shown in Eq. (26), the directional mechanical properties can be obtained using Eq. (8) by inverting $\boldsymbol{Q}(\theta)$ as,

$$\boldsymbol{Q}^{-1}(\theta) = \begin{bmatrix} \frac{1}{Y_1(\theta)} & -\frac{\nu_{21}(\theta)}{Y_2(\theta)} & \frac{\eta_{16}(\theta)}{G(\theta)} \\ -\frac{\nu_{12}(\theta)}{Y_1(\theta)} & \frac{1}{Y_2(\theta)} & \frac{\eta_{26}(\theta)}{G(\theta)} \\ \frac{\eta_{61}(\theta)}{Y_1(\theta)} & \frac{\eta_{62}(\theta)}{Y_2(\theta)} & \frac{1}{G(\theta)} \end{bmatrix}. \tag{28}$$

Fig. 5 shows the directional Young's moduli, shear modulus and Poisson's ratios of rhenium disulfide on polar plots. As can be seen in Fig. 5(a), the Young's modulus in the longitudinal direction is at its maximum value at around $\theta = 1.5°$, whereas the shear modulus is maximum at about $\theta = -22.5°$. Fig. 6 shows the variation of the directional coefficients of mutual influence of rhenium disulfide as the angle θ varies from $-90°$ to $90°$. It is noted that the latter range of variation of the angle θ is sufficient since any angle outside of this range is a $180°$ rotation of an angle within that range which does not affect the properties.

As can be seen in Fig. 6, the coefficients of mutual influence do not collectively vanish under any rotation of the basis. Therefore, it

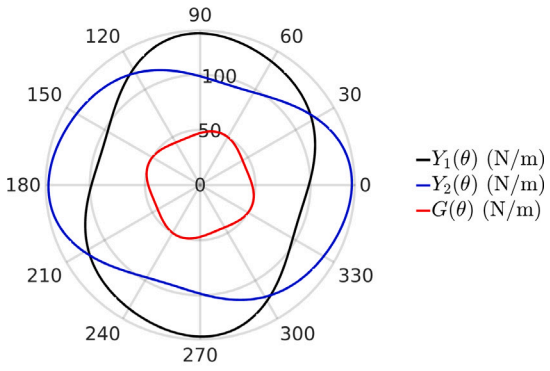

(a) Young's moduli Y_1 and Y_2 and shear modulus G

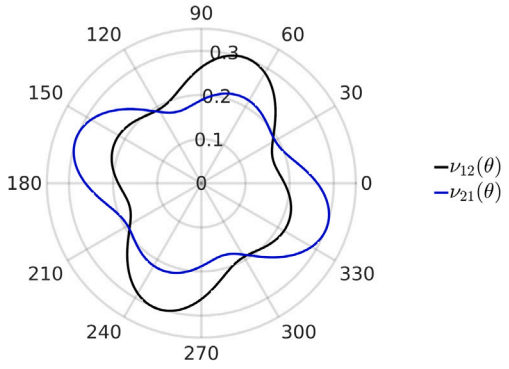

(b) Poisson's ratios ν_{12} and ν_{21}

Fig. 5. Variation of the mechanical properties of rhenium disulfide as the global basis is rotated.

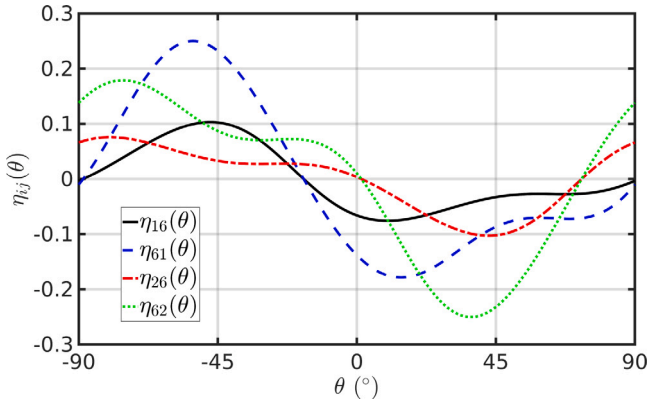

Fig. 6. Variation of the coefficients of mutual influence of rhenium disulfide η_{16}, η_{61}, η_{26} and η_{62} as the global basis is rotated.

is concluded that rhenium disulfide does not act as an orthorhombic material under any rotated configuration.

Using the angles $\theta = \alpha_1 = -0.818°$ and $\theta = \alpha_2 = 0.808°$, we determine the Young's moduli Y_{ξ_1} and Y_{ξ_2} along the unit cell directions $\boldsymbol{\xi_1}$ and $\boldsymbol{\xi_2}$, respectively. These results are presented in Table 5. Since the angle between the $\boldsymbol{e_1}$ and $\boldsymbol{\xi_1}$ directions and that between the $\boldsymbol{e_2}$ and $\boldsymbol{\xi_2}$ directions is less than a degree, i.e., $|\alpha_1|, |\alpha_2| < 1°$, the Young's moduli Y_1 and Y_2 are within 0.4% of Y_{ξ_1} and Y_{ξ_2}, respectively.

7. Comparisons with published work

In this section we compare some of the results presented in this paper with that in the published literature. Refs. [39,60] present results

Table 5
Young's moduli along the rhenium disulfide lattice vectors.

Y_{ξ_1} (N/m)	Y_{ξ_2} (N/m)
98.1	137.4

Table 6
Comparison of some of the elastic properties of rhenium disulfide presented in the current work with that in [39]. The prime denotes elastic properties corresponding to a coordinate system oriented at $\theta = 53.322°$ relative to the $\boldsymbol{e_1}$ direction (cf. Fig. 4).

Study	Q'_{11} (N/m)	Q'_{12} (N/m)	Y'_1 (N/m)	G' (N/m)	ν'_{12}
Current work	135.6	29.9	127.1	49.9	0.269
Ref. [39]	140.8	31.1	133.9	59.4	0.220
Difference (%)	3.8	4.0	5.4	19.0	18.2

for single layer rhenium disulfide along the path of shortest distances between the rhenium atoms, i.e., a rotation corresponding to $\theta = 53.322°$ of the configuration of the current work (cf. Fig. 4). In this section, we will denote the elastic properties with a prime to indicate that they correspond to a coordinate system oriented at $\theta = 53.322°$ relative to the $\boldsymbol{e_1}$ direction (cf. Fig. 4).

Rhenium disulfide has been studied under the assumption that it is a hexagonal 2D material in [39]. Therefore, the results presented in [39] assume higher symmetry than that exhibited by rhenium disulfide. A hexagonal 2D material only possesses 2 linearly independent elastic stiffnesses, e.g., Q_{11} and Q_{12}, which are determined in [39] by curve fitting using the stress–strain curves. While the relations used to evaluate the mechanical properties of rhenium disulfide in [39] correspond to that of a hexagonal material unlike those presented in Eq. (11), the elastic stiffnesses are obtained using a curve fitting approach similar to stress based curve fitting in the current work. Therefore, the values of Q'_{11} and Q'_{12} in [39] can be conclusively compared to that in the current work. The stiffnesses and mechanical properties from [39] are compared to those in the current work in Table 6. As can be seen, the elastic stiffnesses Q'_{11} and Q'_{12} compare well with those from [39]. However, the Young's modulus Y'_1, shear modulus G' and Poisson's ratio ν'_{12} exhibit higher differences due to the hexagonal symmetry assumption. The stiffness Q'_{11} is presented in [60] as $Q'_{11} = 142\,\text{N/m}$, which compares well with the result in the current work and in [39]. Using the elastic stiffnesses from the current work, $Y'_2 = 100.2\,\text{N/m}$ and $\nu'_{21} = 0.212$ but in [39] Y'_2 and ν'_{21} are the same as Y'_1 and ν'_{12} shown in Table 6, respectively, since the material is assumed to be hexagonal.

It is noted that both Refs. [39,60] employed a rhenium disulfide unit cell containing 12 atoms as opposed to 6 atoms as in the current work (cf. Fig. 3(a)). This demonstrates that the periodic unit cell with 6 atoms is sufficient to analyze rhenium disulfide since the elastic stiffnesses Q'_{11} and Q'_{12} in the current work compare well with those from [39,60] (cf. Table 6).

8. Discussion about the anisotropy of rhenium disulfide

As discussed previously, the stiffnesses Q_{16} and Q_{26} of rhenium disulfide do not simultaneously vanish under any rotation of the basis $\{\boldsymbol{e_i}\}$. Therefore, rhenium disulfide never acts as an orthorhombic material. Besides the extension-shear coupling quantified by the Q_{16} and Q_{26}, we can study the degree of anisotropy of rhenium disulfide differently in terms of how closely its directional mechanical properties follow that of an isotropic material. Accordingly, we define the anisotropy index $\mathcal{A}_P$ as follows,

$$\mathcal{A}_P = \frac{P^{\max} - P^{\min}}{\frac{1}{2}\left(P^{\max} + P^{\min}\right)} \times 100\%, \tag{29}$$

where P represents a mechanical property which can either be Y_1, Y_2, G, ν_{12} or ν_{21},

$$P^{\max} = \max_{-90° \le \theta \le 90°} P(\theta) \quad \text{and} \quad P^{\min} = \min_{-90° \le \theta \le 90°} P(\theta). \tag{30}$$

Table 7
Maximum and minimum directional moduli and Poisson's ratios of rhenium disulfide along with the angles at which they occur and the corresponding anisotropy indices $\mathcal{A}_P$.

Elastic modulus P	Extremum	Value	Angle of occurrence θ (°)	Anisotropy index $\mathcal{A}_P$
Y_1	maximum	137.5 N/m	−88.57	37.4%
	minimum	94.2 N/m	−17.22	
Y_2	maximum	137.5 N/m	1.43	
	minimum	94.2 N/m	72.78	
G	maximum	50.6 N/m	−22.50	14.0%
	minimum	44.0 N/m	22.50	
ν_{12}	maximum	0.301	70.70	55.1%
	minimum	0.171	16.96	
ν_{21}	maximum	0.301	−19.30	
	minimum	0.171	−73.04	

It is noted that the anisotropy index $\mathcal{A}_P$ is not defined for the coefficients of mutual influence. The anisotropy index $\mathcal{A}_P$ is independent of the basis used for the analysis. In the case of an isotropic material, the moduli are invariant under rotations, thus, $\mathcal{A}_P^{\text{isotropic}} = 0\%$ since isotropic materials do not exhibit any anisotropy. Table 7 shows the maximum and minimum directional moduli and Poisson's ratios of rhenium disulfide, the angles at which they respectively occur and the corresponding anisotropy indices $\mathcal{A}_P$.

It can be seen in Table 7 that rhenium disulfide exhibits higher anisotropy under axial deformations ($\mathcal{A}_{Y_i}$) as compared to shear ($\mathcal{A}_G$). However, black phosphorus for example is more anisotropic axially since $Y_2 > 4Y_1$ (e.g., see [5]) which corresponds to $\mathcal{A}_Y > 120\%$. It is noted that the anisotropy index is the same for both Young's moduli since Y_2 is a 90° rotation of Y_1. Similarly, in the case of Poisson's ratios, ν_{21} is a 90° rotation of ν_{12} and the anisotropy index takes into account all the rotational range, so both Poisson's ratios share the same anisotropy index.

9. Conclusion

In this paper, we present an approach for determining the elastic stiffnesses of a triclinic 2D material in a global basis. The presented approach can be used to evaluate the mechanical properties of any triclinic 2D material, including the coefficients of mutual influence which relate shear to axial deformations. We illustrate the approach by evaluating the anisotropic plane stress reduced stiffness tensor of triclinic 2D rhenium disulfide. Both the strain energy density and stresses in rhenium disulfide are computed using density functional theory for different strain states and used to curve fit for the elastic stiffnesses. While the stiffnesses obtained using energy based curve fitting are more accurate and satisfy the symmetry requirements, stress based curve fitting is more efficient since it requires fewer density functional theory simulations. We determine the mechanical properties of rhenium disulfide using its stiffness tensor and investigate their directional dependence. It is shown that at no angle do all the coefficients of mutual influence of rhenium disulfide collectively vanish. Therefore, rhenium disulfide always exhibits extension-shear coupling and does not act as an orthorhombic material under any rotation of the global basis. The degree of anisotropy of rhenium disulfide is discussed using the directional elastic moduli.

CRediT authorship contribution statement

Serge R. Maalouf: Conceptualization, Methodology, Software, Validation, Formal analysis, Data curation, Writing – original draft, Writing – review & editing. **Senthil S. Vel:** Conceptualization, Methodology, Software, Validation, Formal analysis, Writing – original draft, Writing – review & editing, Supervision.

Declaration of competing interest

The authors declare that they have no known competing financial interests or personal relationships that could have appeared to influence the work reported in this paper.

Data availability

Data will be made available on request.

Acknowledgments

This research was made possible by the Arthur O. Willey Professorship in Mechanical Engineering. The computational work required for this paper was done in part on the Extreme Science and Engineering Discovery Environment (XSEDE) [61], which is supported by National Science Foundation, under the startup grant TG-PHY210083. The other part of the computational work was done on the University of Maine System Advanced Computing Group (ACG) clusters.

References

[1] D. Akinwande, C.J. Brennan, J.S. Bunch, P. Egberts, J.R. Felts, H. Gao, R. Huang, J.-S. Kim, T. Li, Y. Li, K.M. Liechti, N. Lu, H.S. Park, E.J. Reed, P. Wang, B.I. Yakobson, T. Zhang, Y.-W. Zhang, Y. Zhou, Y. Zhu, A review on mechanics and mechanical properties of 2D materials—Graphene and beyond, Extreme Mech. Lett. 13 (2017) 42–77.

[2] V. Shanmugam, R.A. Mensah, K. Babu, S. Gawusu, A. Chanda, Y. Tu, R.E. Neisiany, M. Försth, G. Sas, O. Das, A review of the synthesis, properties, and applications of 2D materials, Part. Part. Syst. Charact. 39 (6) (2022) 2200031, http://dx.doi.org/10.1002/ppsc.202200031, URL https://onlinelibrary.wiley.com/doi/abs/10.1002/ppsc.202200031.

[3] E. Blundo, E. Cappelluti, M. Felici, G. Pettinari, A. Polimeni, Strain-tuning of the electronic, optical, and vibrational properties of two-dimensional crystals, Appl. Phys. Rev. 8 (2) (2021) 021318, http://dx.doi.org/10.1063/5.0037852.

[4] D.J. Fisher, Rhenium Disulfide, first ed., Materials Research Forum LLC, Millersville, 2018.

[5] S.R. Maalouf, S.S. Vel, Nonlinear elastic analysis of 2D materials of arbitrary symmetries with application to black phosphorus, Mech. Mater. 165 (2022) 104159, http://dx.doi.org/10.1016/j.mechmat.2021.104159.

[6] S.R. Maalouf, S.S. Vel, Nonlinear elastic behavior of 2D materials using molecular statics and comparisons with first principles calculations, Physica E 148 (2023) 115633, http://dx.doi.org/10.1016/j.physe.2022.115633, URL https://www.sciencedirect.com/science/article/pii/S1386947722004568.

[7] X. Wei, B. Fragneaud, C.A. Marianetti, J.W. Kysar, Nonlinear elastic behavior of graphene: Ab initio calculations to continuum description, Phys. Rev. B 80 (2009) 250407.

[8] R.C. Cooper, C. Lee, C.A. Marianetti, X. Wei, J. Hone, J.W. Kysar, Nonlinear elastic behavior of two-dimensional molybdenum disulfide, Phys. Rev. B 87 (2013) 035423.

[9] Q. Peng, High-order nonlinear mechanical properties of g-SiC, Mech. Mater. 148 (2020) 103473.

[10] Q. Zhao, Y. Guo, Y. Zhou, X. Xu, Z. Ren, J. Bai, X. Xu, Flexible and anisotropic properties of monolayer MX2 (M=Tc and Re; X =S, Se), J. Phys. Chem. C 121 (42) (2017) 23744–23751, http://dx.doi.org/10.1021/acs.jpcc.7b07939.

[11] M.E. Kilic, S.E. Rad, S. Ipek, S. Jahangirov, Boron-pnictogens: Highly anisotropic two-dimensional semiconductors for nanoelectronics and optoelectronics, Phys. Rev. Mater. 6 (2022) 064007, http://dx.doi.org/10.1103/PhysRevMaterials.6.064007, URL https://link.aps.org/doi/10.1103/PhysRevMaterials.6.064007.

[12] H. Zhang, Z.-H. Yue, F.-S. Meng, Two-dimensional monolayer B2p6 with anisotropic elastic properties and carrier mobility, Vacuum 195 (2022) 110651, http://dx.doi.org/10.1016/j.vacuum.2021.110651, URL https://www.sciencedirect.com/science/article/pii/S0042207X21005996.

[13] B. Mortazavi, M. Shahrokhi, B. Javvaji, A.V. Shapeev, X. Zhuang, Highly anisotropic mechanical and optical properties of 2D NbOX2 (X= Cl, Br, I) revealed by first-principle, Nanotechnology 33 (27) (2022) 275701, http://dx.doi.org/10.1088/1361-6528/ac622f.

[14] M. Abboud, D.H. Ozbey, M.E. Kilic, E. Durgun, Investigation of anisotropic mechanical, electronic, and charge carrier transport properties of germanium-pnictogen monolayers, J. Phys. D: Appl. Phys. 55 (18) (2022) 185302, http://dx.doi.org/10.1088/1361-6463/ac4cf9.

[15] J. Zhao, W. Wu, J. Zhu, Y. Lu, B. Xiang, S.A. Yang, Highly anisotropic two-dimensional metal in monolayer $MoOCl_2$, Phys. Rev. B 102 (2020) 245419, http://dx.doi.org/10.1103/PhysRevB.102.245419, URL https://link.aps.org/doi/10.1103/PhysRevB.102.245419.

[16] J. Nye, Physical Properties of Crystals, second ed., Oxford Science Publications, New York, 1985.

[17] J. Zhao, D. Ma, C. Wang, Z. Guo, B. Zhang, J. Li, G. Nie, N. Xie, H. Zhang, Recent advances in anisotropic two-dimensional materials and device applications, Nano Res. 14 (2021) 897–919, http://dx.doi.org/10.1007/s12274-020-3018-z.

[18] Z.-d. Gao, Z.-h.-y. Jiang, J.-d. Li, B.-w. Li, Y.-y. Long, X.-m. Li, J. Yin, W.-l. Guo, Anisotropic mechanics of 2D materials, Adv. Eng. Mater. (2022) 2200519, https://doi-org.wv-o-ursus-proxy02.ursus.maine.edu/10.1002/adem.202200519, URL https://onlinelibrary-wiley-com.wv-o-ursus-proxy02.ursus.maine.edu/doi/abs/10.1002/adem.202200519.

[19] M. Yağmurcukardeş, Stable anisotropic single-layer of ReTe2: a first principles prediction, Turk. J. Phys. 44 (2020) 450–457, http://dx.doi.org/10.3906/fiz-2004-17.

[20] M. Yagmurcukardes, C. Bacaksiz, R.T. Senger, H. Sahin, Hydrogen-induced structural transition in single layer ReS_2, 2D Mater. 4 (3) (2017) 035013, http://dx.doi.org/10.1088/2053-1583/aa78c8.

[21] Y. Jiao, L. Zhou, F. Ma, G. Gao, L. Kou, J. Bell, S. Sanvito, A. Du, Predicting single-layer technetium dichalcogenides (TcX2, X=S, Se) with promising applications in photovoltaics and photocatalysis, ACS Appl. Mater. Interfaces 8 (8) (2016) 5385–5392, http://dx.doi.org/10.1021/acsami.5b12606.

[22] R.F.S. Hearmon, The elastic constants of anisotropic materials, Rev. Modern Phys. 18 (1946) 409–440, http://dx.doi.org/10.1103/RevModPhys.18.409, URL https://link.aps.org/doi/10.1103/RevModPhys.18.409.

[23] A. Rabinovich, The elastic constants and the stability of anisotropic materials, in: Proceedings of the Central Aero and Hydrodynamic Institute (Trudy Ts. A. G. I.), vol. 582, 1946.

[24] S. Lekhnitskii, Theory of Elasticity of an Anisotropic Elastic Body, first ed., Holden-Day, Inc., San Francisco, California, 1963.

[25] N.T. Mascia, L. Vanalli, Evaluation of the coefficients of mutual influence of wood through off-axis compression tests, Constr. Build. Mater. 30 (2012) 522–528, http://dx.doi.org/10.1016/j.conbuildmat.2011.12.048, URL https://www.sciencedirect.com/science/article/pii/S0950061811007264.

[26] N. Yang, L. Zhang, Investigation of elastic constants and ultimate strengths of Korean pine from compression and tension tests, J. Wood Sci. 64 (2018) 85–96, http://dx.doi.org/10.1007/s10086-017-1671-y.

[27] M. Faghihnasiri, H. Jafari, A. Ramazani, M. Shabani, S.M. Estalaki, R.G. Larson, Nonlinear elastic behavior and anisotropic electronic properties of two-dimensional borophene, J. Appl. Phys. 125 (14) (2019) 145107.

[28] Q. Peng, C. Liang, W. Ji, S. De, A first-principles study of the mechanical properties of g-GeC, Mech. Mater. 64 (2013) 135–141.

[29] Q. Peng, W. Ji, S. De, Mechanical properties of the hexagonal boron nitride monolayer: Ab initio study, Comput. Mater. Sci. 56 (2012) 11–17.

[30] Q. Peng, W. Ji, S. De, Mechanical properties of graphyne monolayers: a first-principles study, Phys. Chem. Chem. Phys. 14 (38) (2012) 13385–13391.

[31] B. Mousavi, A. Sadeghirad, V. Lotfi, A computational investigation of applicability of nonlinear fracture mechanics in nano-scale fracture of graphene, Mater. Today Commun. 31 (2022) 103687, http://dx.doi.org/10.1016/j.mtcomm.2022.103687, URL https://www.sciencedirect.com/science/article/pii/S2352492822005499.

[32] W.S. Slaughter, The Linearized Theory of Elasticity, first ed., Birkhäuser, Boston, 2002.

[33] D.E. Sands, Introduction to Crystallography, first ed., Dover Publications, Mineola, New York, 1975.

[34] Y.-D. Cao, Y.-H. Sun, S.-F. Shi, R.-M. Wang, Anisotropy of two-dimensional ReS2 and advances in its device application, Rare Met. 40 (2021) 3357–3374, http://dx.doi.org/10.1007/s12598-021-01781-6.

[35] Y. Feng, H. Sun, J. Sun, Y. Shen, Y. You, Probing the low-symmetry structure determined anisotropic elastic properties of rhenium disulphide by first-principle calculations, Mater. Today Commun. 21 (2019) 100684, http://dx.doi.org/10.1016/j.mtcomm.2019.100684, URL https://www.sciencedirect.com/science/article/pii/S2352492819307536.

[36] A. Jain, S.P. Ong, G. Hautier, W. Chen, W.D. Richards, S. Dacek, S. Cholia, D. Gunter, D. Skinner, G. Ceder, K.A. Persson, Commentary: The materials project: A materials genome approach to accelerating materials innovation, APL Mater. 1 (1) (2013) 011002, http://dx.doi.org/10.1063/1.4812323, http://dx.doi.org/10.1063/1.4812323.

[37] M. de Jong, W. Chen, T. Angsten, A. Jain, R. Notestine, A. Gamst, M. Sluiter, C.K. Ande, S. van der Zwaag, J.J. Plata, C. Toher, S. Curtarolo, G. Ceder, K.A. Persson, M. Asta, Charting the complete elastic properties of inorganic crystalline compounds, Sci. Data 2 (2015) 150009, http://dx.doi.org/10.1038/sdata.2015.9.

[38] Materials data on ReS2 by materials project, 2020, http://dx.doi.org/10.17188/1276430, URL https://materialsproject.org/materials/mp-572758/.

[39] H. Sun, P. Agrawal, C.V. Singh, A first-principles study of the relationship between modulus and ideal strength of single-layer, transition metal dichalcogenides, Mater. Adv. 2 (2021) 6631–6640, http://dx.doi.org/10.1039/D1MA00239B, URL http://dx.doi.org/10.1039/D1MA00239B.

[40] P. Agrawal, First Principles Study of Structural-mechanical Property Relationship of Two-dimensional Transition Metal Dichalcogenides and Phosphorene Allotropes (Ph.D. thesis), University of Torronto, 2018, URL https://hdl.handle.net/1807/93150.

[41] E.B. Tadmor, R.E. Miller, Modelling Materials: Continuum, Atomistic and Multiscale Techniques, first ed., Cambridge University Press, Cambridge UK, 2016.

[42] A. Kokalj, XCrySDen—a new program for displaying crystalline structures and electron densities, J. Mol. Graph. Model. 17 (3) (1999) 176–179, http://dx.doi.org/10.1016/S1093-3263(99)00028-5.

[43] W. Voigt, Lehrbuch Der Kristallphysik, B.G. Teubner, Berlin, 1910.

[44] F. Murnaghan, Finite deformations of an elastic solid, Am. J. Math. 59 (1937) 235–260.

[45] Y. Hiki, Higher order elastic constants of solids, Annu. Rev. Mater. Sci. 11 (1) (1981) 51–73.

[46] P. Hohenberg, W. Kohn, Inhomogeneous electron gas, Phys. Rev. B 136 (1964) B864–B871.

[47] W. Kohn, L. Sham, Self-consistent equations including exchange and correlation effects, Phy. Rev. A 140 (1965) A1133–A1138.

[48] G.H. Golub, C.F. Van Loan, Matrix Computations, third ed., Johns Hopkins University Press, Baltimore, 1996.

[49] N.J. Higham, Functions of Matrices: Theory and Computation, first ed., SIAM, Philadelphia, 2008.

[50] C.L. Lawson, R.J. Hanson, Solving Least Squares Problems, Prentice Hall, Englewood, 1974.

[51] G. Strang, Introduction To Applied Mathematics, first ed., Wellesley-Cambridge Press, Wellesley, 1986.

[52] P. Giannozzi, O. Andreussi, T. Brumme, O. Bunau, M.B. Nardelli, M. Calandra, R. Car, C. Cavazzoni, D. Ceresoli, M. Cococcioni, N. Colonna, I. Carnimeo, A.D. Corso, S. de Gironcoli, P. Delugas, R.A.D. Jr, A. Ferretti, A. Floris, G. Fratesi, G. Fugallo, R. Gebauer, U. Gerstmann, F. Giustino, T. Gorni, J. Jia, M. Kawamura, H.-Y. Ko, A. Kokalj, E. Küçükbenli, M. Lazzeri, M. Marsili, N. Marzari, F. Mauri, N.L. Nguyen, H.-V. Nguyen, A.O. de-la Roza, L. Paulatto, S. Poncé, D. Rocca, R. Sabatini, B. Santra, M. Schlipf, A.P. Seitsonen, A. Smogunov, I. Timrov, T. Thonhauser, P. Umari, N. Vast, X. Wu, S. Baroni, Advanced capabilities for materials modelling with QUANTUM ESPRESSO, J. Phys.: Condens. Matter 29 (46) (2017) 465901, URL http://stacks.iop.org/0953-8984/29/i=46/a=465901.

[53] P. Giannozzi, S. Baroni, N. Bonini, M. Calandra, R. Car, C. Cavazzoni, D. Ceresoli, G.L. Chiarotti, M. Cococcioni, I. Dabo, A. Dal Corso, S. de Gironcoli, S. Fabris, G. Fratesi, R. Gebauer, U. Gerstmann, C. Gougoussis, A. Kokalj, M. Lazzeri, L. Martin-Samos, N. Marzari, F. Mauri, R. Mazzarello, S. Paolini, A. Pasquarello, L. Paulatto, C. Sbraccia, S. Scandolo, G. Sclauzero, A.P. Seitsonen, A. Smogunov, P. Umari, R.M. Wentzcovitch, QUANTUM ESPRESSO: a modular and open-source software project for quantum simulations of materials, J. Phys.: Condens. Matter 21 (39) (2009) 395502, (19pp), URL http://www.quantum-espresso.org.

[54] P. Blöchl, Projector augmented-wave method, Phys. Rev. B 50 (24) (1994) 17953–17979.

[55] J.P. Perdew, K. Burke, M. Ernzerhof, Generalized gradient approximation made simple, Phys. Rev. Lett. 77 (18) (1996) 3865–3868.

[56] H.J. Monkhorst, J.D. Pack, Special points for brillouin-zone integrations, Phys. Rev. B 13 (12) (1976) 5188–5192, http://dx.doi.org/10.1103/PhysRevB.13.5188.

[57] H.H. Murray, S.P. Kelty, R.R. Chianelli, C.S. Day, Structure of rhenium disulfide, Inorg. Chem. 33 (19) (1994) 4418–4420, http://dx.doi.org/10.1021/ic00097a037.

[58] O.H. Nielsen, R.M. Martin, Quantum-mechanical theory of stress and force, Phys. Rev. B 32 (6) (1985) 3780–3791.

[59] W.L. Bond, The mathematics of the physical properties of crystals, Bell Syst. Tech. J. 22 (1) (1943) 1–72, http://dx.doi.org/10.1002/j.1538-7305.1943.tb01304.x, URL https://onlinelibrary.wiley.com/doi/abs/10.1002/j.1538-7305.1943.tb01304.x.

[60] S. Yu, H. Zhu, K. Eshun, C. Shi, M. Zeng, Q. Li, Strain-engineering the anisotropic electrical conductance in ReS2 monolayer, Appl. Phys. Lett. 108 (19) (2016) 191901, http://dx.doi.org/10.1063/1.4947195.

[61] J. Towns, T. Cockerill, M. Dahan, I. Foster, K. Gaither, A. Grimshaw, V. Hazlewood, S. Lathrop, D. Lifka, G.D. Peterson, R. Roskies, J.R. Scott, N. Wilkins-Diehr, XSEDE: Accelerating scientific discovery, Comput. Sci. Eng. 16 (5) (2014) 62–74, http://dx.doi.org/10.1109/MCSE.2014.80, URL http://doi.ieeecomputersociety.org/10.1109/MCSE.2014.80.